NASA TECHNICAL MEMORANDUM

NASA TM X-52201

NASA TM X-52201

SOLAR-ELECTRIC PROPULSION SYSTEM PERFORMANCE FOR THE 0.1-AU SOLAR PROBE MISSION

by William C. Strack
Lewis Research Center
Cleveland, Ohio

TECHNICAL PAPER proposed for presentation at
West Coast Aerospace Sciences Meeting sponsored
by the American Institute of Aeronautics and Astronautics
Los Angeles, California, June 27-29, 1966

NATIONAL AERONAUTICS AND SPACE ADMINISTRATION · WASHINGTON, D.C. · 1966

SOLAR-ELECTRIC PROPULSION SYSTEM PERFORMANCE FOR THE O. 1-AU SOLAR PROBE MISSION

by William C. Strack

Lewis Research Center
Cleveland, Ohio

TECHNICAL PAPER proposed for presentation at

West Coast Aerospace Sciences Meeting
sponsored by the American Institute of Aeronautics and Astronautics
Los Angeles, California, June 27-29, 1966

NATIONAL AERONAUTICS AND SPACE ADMINISTRATION

SOLAR-ELECTRIC PROPULSION SYSTEM PERFORMANCE FOR THE 0.1-AU SOLAR PROBE MISSION

by William C. Strack*

Lewis Research Center
National Aeronautics and Space Administration
Cleveland, Ohio

E-3040

ABSTRACT

Saturn IB/Centaur and Atlas/Centaur launched electric propulsion vehicles employing present or near-future state-of-the-art power supplies (50 to 100 lb/kW_e) are shown to be attractive systems for performing the 0.1-AU solar probe mission. This result compares favorably with the alternative systems composed of the same boosters but with chemical or nuclear final stages - which are inadequate for this mission. The performance calculations for the electric propulsion systems include the optimization of the launch vehicle burnout velocity, the electric stage specific impulse and power level, and the thrust orientation for constant specific impulse thrustors. Two sets of results are presented. The first set is associated with constant power operation of the thrustors as would be the case for nonsolar dependent power supplies such as nuclear-electric systems. The second set of data represents solar-cell-powered electric systems. In this case the thrustor power is a function of the sun-vehicle distance. The power is varied by adjustment of the propellant flow rate. Of special interest is the fact that absolute optimal trajectories for the solar cell systems belong to an entirely different class than those optimals associated with constant power systems.

*Aerospace Research Engineer

TM X-52201

NOMENCLATURE

a_o	initial acceleration of electric stage, ft/sec^2
$G(r)$	power profile function
g_o	32.174 ft/sec^2
I_c	specific impulse of chemical stage, sec
I_e	specific impulse of electric stage, sec
K	hardware fraction of chemical stage
k	ratio of tankage to propellant mass of electric stage
M_h	hardware mass (propellant tanks, engines, structure, etc.) of chemical stage, lb
M_o	initial mass of vehicle in circular Earth orbit, lb
M_p	propellant mass of chemical stage, lb
m_f	final mass, lb
m_L	payload mass, lb
m_o	initial mass of electric stage, lb
m_p	propellant mass of electric stage, lb
m_{pp}	powerplant mass of electric stage, lb
m_s	structure mass of electric stage, lb
m_t	tankage mass of electric stage, lb
P	total power delivered to electric thrustors, kW
r	heliocentric radius, AU
r_o	initial circular Earth-orbit radius, ft
r_s	radius of sphere of influence, ft
V_b	chemical stage burnout velocity, ft/sec
V_c	circular Earth-orbit velocity, ft/sec

V_e escape velocity (valuc of V_b that results in $V_s = 0$), ft/sec

V_o initial heliocentric velocity, ft/sec

V_s velocity at r_s, ft/sec

$V_\oplus$ Earth's heliocentric velocity, ft/sec

α overall specific mass of electric powerplant (including power conditioning and ion engine system) at 1.0 AU, lb/kW_e

η thrustor efficiency

μ gravitational constant of the Sun, ft^3/sec^2

φ terminal configuration angle between Sun-probe line and Sun-Earth line, deg

Subscript

opt optimum

INTRODUCTION

Inasmuch as the Sun is unquestionably the very basis of our solar system and since it is the predominate factor controlling the environment of the solar system, it is quite important that new scientific knowledge be found about this "center of attraction." However, Earth-based solar studies are severely hampered by the protective atmospheric and electromagnetic shields surrounding the Earth. Of course, some solar study has been and will continue to be carried out by interplanetary probes and orbiting solar observatories. But several of the important proposed solar experiments (corona radar sounding, ultraviolet and X-ray spatial resolution of the solar disk, determining the connection between the rotating solar corona and the solar wind, etc.) require close-in solar probes; that is, probes whose perihelion radii are on the order of 0.1 AU.[1,2] This paper analyzes vehicle systems capable of accomplishing

this mission (with emphasis on the solar-cell-powered electric system) rather than the solar experiments or the scientific payloads required to perform them.

The major conclusion regarding all high-thrust propulsion for the 0.1 AU solar fly-by probe mission[3 to 5] is that only very small payload fractions (if any at all) are realizable. In particular, both the all chemical Saturn IB/Centaur/kick stage and the Saturn IB/nuclear ($1\frac{1}{2}$ stages) launch vehicles cannot deliver any payload on a 0.1 AU perihelion radius trajectory. It is true that Saturn V boosters with additional high-energy chemical upper stages or a nuclear upper stage can forcibly deliver some payload for this mission, but the payload fractions are still unattractively small and such systems are at least a decade from becoming operational.

As is usually the case when high-thrust propulsion capabilities are pressed close to their limits, interest in electric-propulsion systems is stimulated. Past electric-propulsion studies[6 to 8] for this mission have, however, assumed rather advanced technology - either by choosing quite low values (e.g., 10 to 30 lb/kW_e) of the overall specific powerplant mass α or by assuming a large Saturn V/nuclear-electric system. A recent report[9] by the present author presented variational results for this mission that showed that chemical-electric hybrid systems offered attractive capability even with present and near future power-supply technology (i.e., Saturn IB/Centaur/electric vehicles were assumed, with α = 10-150 lb/kW_e). These results were generated with electric power held constant. Other recent studies[10,11] have shown that lightweight solar-cell power supplies can be manufactured using current technology with α's on the order of 50 lb/kW_e.

Since the power output of a solar cell varies with the distance from the sun, the results of Ref. 9 are not applicable to the case of solar-cell powered probes. The constant power optimal trajectories of interest reported in Ref. 9 would cause the vehicle to spend the major portion of its trip at considerable distances outside of the Earth's orbit. Hence, solar-powered vehicles might be expected to suffer severe performance penalties when compared with like constant power vehicles. With the intent to clarify this, the present paper concerns itself primarily with solar-cell-powered solar flyby probes.

Also, the great potential of electric propulsion for the 0.1 AU-solar-probe mission by using current state-of-the-art technology is demonstrated. Naturally, a multitude of systems integration problems should be considered for any new type of spacecraft design. A survey of such problems is contained in Ref. 12. An in-depth investigation into such design areas as accommodation of the changing solar array output to the engines, and deployment and orientation of the solar array for a Mars orbiter mission by using solar electric propulsion is reported in Ref. 13.

ANALYSIS

The analysis presented below is concerned with determining the performance of electric-powered solar flyby probes. Rather than repeat analyses already reported for chemical and nuclear powered systems, results for these systems will be taken from other studies as required. The primary performance criterion is the payload ratio. The electric stage is assumed to start either in an initial circular 100-nautical-mile Earth orbit or in heliocentric space after a chemical boost out of the reference orbit. These two cases are referred to as the all electric and chemical-electric hydrid systems, respec-

tively. The optimization of the amount of chemical velocity addition beyond the reference point would require solutions to the three-body variational problem whenever the chemical boost velocity were less than escape velocity. Such solutions are quite difficult to obtain from a computational standpoint; therefore, the chemical boost velocities were restricted to values at least as large as escape velocity.

Chemical-electric hybrid system. - The mathematical problem for the hybrid system may be stated as follows: given a mission time and specific-power powerplant mass, determine the maximum payload ratio achievable with a continued firing of the initial launch vehicle and an electric final stage by finding the optimum trajectory, chemical stage burnout velocity, electric stage specific impulse and initial acceleration. In order to avoid the complex calculations involved in the three-body variational problem as discussed here, three assumptions were made: (1) the chemical stage is fired until at least escape velocity is attained; (2) the gravitational effect of the Sun is negligible during the chemical stage of the flight, while the gravitational effect of the Earth is negligible during the electric stage of the flight, and (3) the time elapsed between chemical stage burnout and sphere of influence penetration is negligible.

The thrust vector control of the heliocentric phase is determined by variational principles. This statement means that (1) the Euler-Lagrange equations are employed for the determination of the electric thrustor orientation, (2) the transversality relations are used to optimize the heliocentric travel angle and Earth escape velocity orientation, and (3) the coast phases are optimized.

The payload equation for the chemical-electric hybrid system just described may be written

$$\frac{m_L}{M_o} = \frac{m_o}{M_o}\left(1 - \frac{m_p}{m_o} - \frac{m_{pp}}{m_o} - \frac{m_t}{m_o} - \frac{m_s}{m_o}\right) \tag{1}$$

where m_o/M_o is the payload ratio of the chemical stage from Earth orbit and the sum of terms enclosed in parentheses represents the payload ratio of the electric stage. In order to facilitate the discussion concerning the maximization of the payload ratio m_L/M_o equation (1) will be rewritten in terms of the pertinent problem variables (specific impulse, initial acceleration, etc.).

The tankage mass of the electric stage m_t is usually taken to be proportional to the propellant mass of the electric stage m_p. Thus, if k is the proportionality constant,

$$m_t = km_p \tag{2}$$

Defining the overall specific powerplant mass α to be the ratio of the powerplant mass (including power conditioning and ion engine system) at 1.0 AU divided by the power supplied to the thrustors P and defining the thrustor efficiency η to be the ratio of the propulsive power divided by the total power supplied to the thrustors result in the powerplant mass fraction being rewritten as

$$\frac{m_{pp}}{m_o} = \frac{P}{m_o}\,\alpha = \frac{a_o I_e g_o}{47.47\times10^3}\,\frac{\alpha}{\eta} \tag{3}$$

where a_o is the initial acceleration of the electric stage, I_e is the specific impulse of the electric stage, and 47.47×10^3 is a constant that is required for the system of units employed in this paper.

The payload mass of the chemical stage (initial mass of the electric stage) can be written as

$$m_o = M_o - M_p - M_h$$

where the hardware mass M_h is composed of such things as tankage mass,

engine mass, guidance and control mass, and structure mass. For chemical rockets, the hardware mass can usually be taken to be proportional to the propellant mass M_p. If K is the hardware proportionality constant, then

$$M_h = KM_p \tag{4}$$

If the chemical stage imparts an impulsive velocity change from circular orbit velocity V_c to burnout velocity V_b the chemical stage payload ratio is given by

$$\frac{m_o}{M_o} = (1 + K)e^{-(V_b - V_c)/I_c g_o} - K \tag{5}$$

If equations (2) to (5) are substituted into equation (1) along with the final mass relation $m_f = m_o - m_p$, there results

$$\frac{m_L}{M_o} = \left[(1 + K)e^{-(V_b - V_c)/I_c g_o} - K\right]\left[(1 + k)\frac{m_f}{m_o} - \frac{a_o I_e g_o}{47.47 \times 10^3}\frac{\alpha}{\eta} - \left(k + \frac{m_s}{m_o}\right)\right] \tag{6}$$

This equation is the final form of the function to be maximized. The electric stage final mass ratio m_f/m_o increases as a_o, I_e, and V_b are increased. However, increases in a_o and I_e also increase m_{pp}/m_o, while increasing V_b decreases m_o/M_o. Clearly, there exist values of a_o, I_e, and V_b that will result in a maximum payload ratio. These three variables were optimized by a three-dimensional search scheme.

The maximization of m_f/m_o can be formulated as a Mayer problem in the calculus of variations wherein mission time is treated as a parameter and the constraints are composed of the two-dimensional equations of motion plus some constraint on the electric engine operation. In the case of constant power this latter constraint was chosen to be either maximum thrust or no thrust (coasting flight). In the more general case where power is some function $G(r)$ of the radius, the constraint was chosen to be either no thrust or thrust directly proportional to $G(r)$, where the variation is accomplished by adjusting the propellant flow rate while holding the specific impulse constant. (Actually, $G(r)$ is defined to be the ratio of the power at radius r to the

power at $r = 1.0$ AU.) The solution to the Euler-Lagrange variational equations with an arbitrary power profile $G(r)$ included is given in Appendix A. Constant power operation is just a special case of this formulation in which $G(r) = 1$. For this study, the heliocentric travel angle is left unspecified (free for optimization). Another boundary condition that is not completely specified is the initial heliocentric velocity V_o, which is obtained by vectorially adding the velocity relative to the Earth at the sphere of influence V_s to the Earth's orbital velocity about the Sun $V_\oplus$ as shown in Fig. 1. The optimum orientation of V_s is in the direction of the initial electric thrust vector as can be shown by the transversality condition of the Mayer formulation. The magnitude of V_s is related to the burnout velocity V_b by the conservation of energy as follows:

$$V_s = \sqrt{V_b^2 - 2V_c^2\left(1 - \frac{r_o}{r_s}\right)} \tag{7}$$

For this study, the sphere of influence radius r_s was taken to be 120 Earth radii.

Defining the thrustor efficiency is necessarily somewhat approximate because the functional relation $\eta(I_e)$ (e.g., fig. 2) is dependent on the thrustor employed and its state of development. The bulk of the data was calculated for electron bombardment thrustors by using the efficiency function displayed in Fig. 2. After the constants V_c, I_e, K, k, and m_s/m_o are assigned values (see table I), the payload ratio as given in Eq. (6) may be maximized by a three-dimensional search on V_b, a_o, and I_e over the class of optimal heliocentric trajectories for any given pair of mission time and α. Since V_b is constrained to take on values at least as large as the escape velocity V_e, it might be expected that the optimum V_b could fall exactly on this limit (i.e., $V_{b,opt} = V_e$). Ref. 9 shows, however, that the mathematical model that has been created for the hybrid system prevents $V_{b,opt}$ from becoming less than or equal to V_e.

All electric system. - The payload maximization scheme for the all electric system may be performed similarly to the hybrid system scheme. The booster burnout velocity V_b is not involved so that only two variables (a_o and I_e) need be optimized by the search scheme. Optimum Earth-escape trajectories for low-thrust vehicles are very nearly tangential thrust spirals that can be quite accurately computed in closed form. In this case, the ratio m_o/M_o in Eq. (1) is unity; and the Earth-escape spiral propellant mass and time were computed from the equations in Ref. 9 that were developed in Ref. 14.

The solar cell power function G(r). - The output power of solar cells undergoes changes during the flight due to the following circumstances (1) the solar energy flux varies as the inverse square of the radius, (2) the solar cell efficiency is a decreasing function of temperature, and (3) the incidence angle of the flux with the array surface may change. Normally, the latter factor is not particularly important, since, for most radii, an array perpendicular to the flux produces maximum power. But solar cell temperature increases as the radius decreases, and there exists a radius below which the temperature function dominates over the flux function, which causes power output to fall rapidly. At radii smaller than the maximum power radius, however, the array may be tipped at such an angle so as to keep the power constant at its maximum value. The tip angle may be increased as radius decreases until the back face of the solar panel array is exposed to the Sun (the size of the Sun must be considered at small radii). If the radius is allowed to fall below this limiting point, the power will fall rapidly to zero. The power profile G(r) used in this study is derived in Appendix B and displayed in Fig. 3. Matching the propulsion system load to the changing solar array output power and voltage characteristics can be accomplished by changing the number of operable thrustors at selected time points and by continual adjustment of the propellant flow rate per thrustor. A detailed analysis of this method of power

matching is reported in Ref. 13.

CONSTANT POWER PERFORMANCE

The payload delivered to 0.1 AU by a Saturn IB/Centaur/electric stage vehicle is displayed in Fig. 4 as a function of mission time and specific powerplant mass. The family of curves representing the hybrid systems do not blend smoothly into the all electric curves because of the restrictive assumption requiring V_b to be at least escape velocity. (A fuller discussion appears in Ref. 9.) The results include three types of electric engine clusters: (1) 10-cm-diameter, electron-bombardment engine clusters, (2) 50-cm-diameter, electron-bombardment engine clusters, and (3) electrothermal engine clusters. The characteristic efficiency curves for these engine types are shown in Fig. 2. The gain in efficiency due to increased thrustor size is reflected by a substantial performance increase. The performance of the electrothermal engines is inferior to that of the electron-bombardment engines because of the unfavorable efficiency curve. Each point on Fig. 4 has been optimized with respect to V_b and I_e. Only the circled points include the optimization with respect to a_o. The other points all lie on curves representing all propulsion operation (no coast). It is evident that very little payload benefit results from coasting trajectories - thus justifying the selection of all propulsion trajectories throughout much of this paper. Two simplifications arise from this constraint: (1) the boundary-value problem associated with the variational problem becomes much less sensitive, and, therefore, the iterative method of solution converges faster, and (2) a_o is no longer a variable that needs to be optimized; instead, it is determined by the associated boundary-value problem.

Two typical trajectories of the constant power hybrid system are shown in Fig. 5. Arrows denoting optimal thrust direction are placed on the trajectory at equal time increments. Trajectory A is of greatest interest since it represents an optimal trajectory for the necessarily long mission time trips of high

specific powerplant mass systems. It is evident from the trajectory diagram that the long missions are characterized by an initial phase that moves the vehicle to a high radius (and accompanying low velocity) and a terminal phase that simply removes angular momentum.

SOLAR CELL POWER PERFORMANCE

The constant power trajectories associated with the systems of major interest (α = 50 to 100 lb/kW_e) lie well outside of the Earth's orbit. Admittedly, the inclusion of the solar cell power profile presupposes either a major performance decrease or a marked alteration of the trajectory to counter the effect of a decreasing power profile. The former can be noted in Fig. 6 where reduced payloads resulting from using G(r) of Fig. 3 and trajectories differing but little from trajectories of constant power are shown by the dashed lines. The latter expectation prompted a search for a different class of optimal trajectories that would produce higher payloads. Such a class of optimal trajectories was indeed discovered. The new class of optimals is characterized by inward paths of $2\frac{1}{2}$ revolutions about the Sun. A representative trajectory from the $2\frac{1}{2}$ revolution class optimals is shown in Fig. 7 where thrust pointers have also been included. Varying trip time from 400 to 500 days produced only about 0.2 degree difference in optimal heliocentric travel angle (905°). This fact leads to a corollary; namely, that a set of optimal classes probably exists, each class characterized by the number of revolutions $N + \frac{1}{2}$ (N an integer) about the Sun. The class that is globally optimal would be primarily a function of trip time. In any event, the present study was restricted to the $2\frac{1}{2}$ revolution class optimals.

Before discussing the payloads associated with these trajectories, a few additional comments concerning the nature of these inward trajectories should be made. An important parameter in communication studies of solar probes is the angle φ between the Sun-Earth radius and the Sun-probe radius. The Sun

is a powerful source of background noise, and this creates a communications blackout region when φ is near 0° or 180°. The value of φ at perihelion is most critical for the solar probe since this is where the major data is to be gathered. The values of φ at the three perihelia for the 400 day trip shown on Fig. 7 are about 105°, 90°, and 150°, which are perfectly acceptable. Increasing the mission time to 450 days would cause all three φ values to be within 15° of 90°, an ideal situation from the communications standpoint.

Another point of interest is the favorable locations of the three optimum coast phases. Since these are centered at the perihelia and extend to about 0.3 AU, the power normally required by the electric propulsion system becomes available to the scientific payload and communications system at a time when these systems would benefit most from a substantial power boost. This factor can be of considerable importance when comparing electric systems with chemical and nuclear systems for missions of high electric power requirements. In such cases, electric systems do not need to carry along a separate power supply as do the high thrust systems.

The payloads associated with the $2\frac{1}{2}$ revolution inward trajectories are represented as solid curves in Fig. 6. The inward trajectories show a very large increase in payload over the outward trajectories. (This is not true in the case of constant power.) A comparison between the optimum constant power case (outward trajectories) and the optimum solar cell power case (inward trajectories) can be made by using the top four curves in this figure. Clearly, neither case is always superior to the other, but as a general rule, solar cell power will deliver more payload than constant power at sufficiently high α or sufficiently low mission time. In particular, for 400 day missions, solar cell power delivers more payload if α is greater than 65 lb/kW_e. In addition to the Saturn IB/Centaur launch vehicle capability shown in Fig. 6, the payloads achievable with an Atlas/Centaur launch vehicle are also shown for the case of

solar cell power. The circled point on Fig. 6 represents the coasting trajectory of Fig. 7 (the curves represent all propulsion) using solar cell power and shows that, as in the case of constant power, a small payload benefit results from the use of coast phases.

According to several recent studies[12,13] overall solar cell specific powerplant masses of 75 lb/kW_e are within the realm of current state-of-the-art technology. With this in mind, a summary of system performance and design parameters for chemical, nuclear, and electric final stages atop Saturn IB/Centaur and Atlas/Centaur launch vehicles is presented in table II for α = 75 lb/kW_e. The all chemical system data and the $1\frac{1}{2}$ stage nuclear system data is presented only at the 75-day mission time since this time represents a minimum energy transfer. Neither of these high thrust systems can deliver positive payloads. (This data is taken from an unpublished study by the Advanced Development and Evaluation Division at the Lewis Research Center and Ref. 7.) Likewise, the all electric system (no chemical boost out of the initial circular orbit) cannot deliver positive payloads. Only the chemical-electric hybrid system can achieve a 0.1 AU perihelion radius with a positive payload. If a larger, more efficient launch vehicle were assumed (e.g., Saturn V), chemical propulsion alone could deliver some payload[7], but by the same token, the hybrid system's payloads would increase correspondingly. The nuclear rocket system is similar to the chemical system in that larger boosters are necessary to provide positive payloads. Besides, nuclear rocket systems do not fall into the near future category. Clearly, if both Saturn V class boosters and nuclear rockets were available, the nuclear-electric hybrid (instead of the chemical-electric hybrid) should be compared with the nuclear system.

CONCLUDING REMARKS

To accomplish the 0.1 AU solar flyby mission starting from an initial circular Earth orbit, a hybrid system consisting of high-thrust and low-thrust

stages offers distinct advantages over either system separately. All chemical systems are quite unattractive for the close solar probe mission in view of their very small payload ratios. All electric propulsion out of a low circular Earth orbit is also unattractive unless overall specific powerplant masses of less than 50 lb/kW_e become available. Electric propulsion systems boosted to hyperbolic velocities, however, can deliver significant payloads with the relatively high values of α characteristic of the current state-of-the-art technology of solar cell power supplies. For instance, a Saturn IB/Centaur/solar electric vehicle with an overall specific powerplant mass of 75 lb/kW_e could deliver a 1310 lb payload to 0.1 AU in 400 days, or a 1850 lb payload in 500 days.

A more detailed analysis would be required for an in-depth systems design. Fig. 7 of the text for example, reveals that a reverse circumferential thrust program (simpler to employ) would be nearly as good as an optimal thrust program. The present analysis is sufficient, however, to show that current state-of-the-art solar electric propulsion is quite attractive for the 0.1 AU solar flyby mission in terms of payload capacity, favorable communications angles, and the possible use of the propulsion power supply to act also as the power supply of the payload package and communications systems at the perihelia.

APPENDIX A - VARIATIONAL EQUATIONS FOR RADIUS DEPENDENT POWER

An analysis of the variational problem is not presented here. Instead, only the final equations are listed as extensions of those derived in Ref. 15 for the constant power case. Although the calculations in this paper were carried out in two dimensions, the solution of the three dimensional case is given here for completeness. The problem is to find the thrust program that minimizes the fuel consumption for a transfer trajectory satisfying specific initial and final conditions, where the specific impulse is held fixed and the

propellant flow rate varies as $G(r)$ if the engines are turned on or is zero if the engines are turned off. Let x, y, and z be rectangular position coordinates and u, v, w the corresponding velocity components in a Cartesian coordinate system. Let m be the mass of the vehicle, c the exhaust velocity, and β_{max} the propellant flow rate at $r = 1.0$ AU for engine-on operation. Then the solution to the stated problem is given by the following set of first order differential equations, where differentiation with respect to time is denoted by a superscript dot.

$$\dot{u} = - \Phi_x + \frac{c\beta_o}{m} G(r) \frac{\lambda_1}{\Lambda}$$

$$\dot{v} = - \Phi_y + \frac{c\beta_o}{m} G(r) \frac{\lambda_2}{\Lambda}$$

$$\dot{w} = - \Phi_z + \frac{c\beta_o}{m} G(r) \frac{\lambda_3}{\Lambda}$$

$$\dot{x} = u \qquad\qquad \dot{\lambda}_1 = -\lambda_4$$

$$\dot{y} = v \qquad\qquad \dot{\lambda}_2 = -\lambda_5$$

$$\dot{z} = w \qquad\qquad \dot{\lambda}_3 = -\lambda_6$$

$$\dot{\lambda}_4 = \lambda_1\Phi_{xx} + \lambda_2\Phi_{yx} + \lambda_3\Phi_{zx} - G'(r)\beta_o K \frac{x}{r}$$

$$\dot{\lambda}_5 = \lambda_1\Phi_{xy} + \lambda_2\Phi_{yy} + \lambda_3\Phi_{zy} - G'(r)\beta_o K \frac{y}{r}$$

$$\dot{\lambda}_6 = \lambda_1\Phi_{xz} + \lambda_2\Phi_{yz} + \lambda_3\Phi_{zz} - G'(r)\beta_o K \frac{z}{r}$$

$$\dot{\lambda}_7 = \frac{c\beta_o}{m} G(r)\, \Lambda$$

$$\dot{m} = -\beta_o G(r)$$

where

$$\Phi = - \frac{\mu}{r}$$

$$\Phi_{xy} = \frac{\partial^2 \Phi}{\partial x\, \partial y} = - \frac{3\mu}{r^5} xy \qquad x \to y, z$$

$$\Phi_{xx} = \frac{\partial^2 \Phi}{\partial x^2} = \frac{\mu}{r^3}\left[1 - 3\left(\frac{x}{r}\right)^2\right] \qquad y \to x, z$$

$$\Lambda = \sqrt{\lambda_1^2 + \lambda_2^2 + \lambda_3^2}$$

$$r = \sqrt{x^2 + y^2 + z^2}$$

$$K = \frac{c\Lambda}{m} - \lambda_7$$

$$c = g_o I_e$$

$$G'(r) = \frac{dG}{dr}$$

$$\beta_o \begin{cases} = 0 & \text{if } K < 0 \\ = \beta_{max} & \text{if } K > 0 \end{cases}$$

APPENDIX B - SOLAR CELL POWER PROFILE*

An isolated flat plate solar panel at distance r from the Sun is considered where r is large enough to assume that the solar flux lines are parallel. If the panel is inclined at an angle i to the solar flux lines and is at the equilibrium temperature T, then for equilibrium conditions the absorbed power is equal to the sum of the radiated power and the electrical output power, that is,

$$\left(\alpha_c + \frac{1 - z}{z}\alpha_f\right)\frac{I}{r^2}\sin i = \left(\epsilon_c + \frac{1 - z}{z}\epsilon_f + \frac{\epsilon_b}{z}\right)\sigma T^4 + \eta(T)\frac{I}{r^2}\sin i \qquad (B1)$$

where α is the absorptivity, ϵ is the emissivity, z is the packing factor, σ is the Stefan-Boltzmann constant, I is the solar flux intensity at 1 AU, $\eta(T)$ is the temperature dependent solar cell efficiency, and the subscripts c, f, and b refer to cell area, front (toward the Sun) noncell area, and back area, respectively. Solving equation (B1) for T yields

$$T = \left(\frac{I}{\sigma}\frac{\alpha_c + \frac{1 - z}{z}\alpha_f}{\epsilon_c + \frac{1 - z}{z}\epsilon_f + \frac{\epsilon_b}{z}}\right)^{1/4}\left(\frac{\sin i}{r^2}\right)^{1/4}\left(1 - \frac{\eta(T)}{\alpha_c + \frac{1 - z}{z}\alpha_f}\right)^{1/4} \qquad (B2)$$

For temperatures between 150° and 500° K, the last factor of this equation ranges between 0.95 and 1.0, and is therefore assumed to be 1.0 in this simple analysis. The resulting maximum temperature error is about 10° K at T = 250° K.

*This derivation was derived by Charles Zola of the NASA Lewis Research Center.

The first factor of this equation can be reduced to a constant by assigning values to the surface properties. For silicon solar cell panels, the following values were assumed: $\alpha_c = 0.94$, $\epsilon_c = 0.875$, $z = 0.95$, $\alpha_f = 0.1$, $\epsilon_f = 0.1$, $\epsilon_b = 0.96$, $I = 130$ W/ft^2, and $\sigma = 0.527 \times 10^{-8}$ W/ft^2/°K^4. Then equation (B2) is simplified to:

$$T = 333 \frac{(\sin i)^{1/4}}{\sqrt{r}} \text{ °K} \tag{B3}$$

Further, Ref. 16 shows that $\eta(T)$ is nearly linear over the temperature range 150° to 500° K. Thus, if η_o is the cell efficiency at $T = 298°$ K, $\eta(T)$ is

$$\eta(T) = \eta_o + \frac{d\eta}{dT} (T - 298) \tag{B4}$$

If the data of Fig. 8 in Ref. 16 is used, $\eta_o = 0.10$, $d\eta/dT = -0.00046°\ K^{-1}$, and hence,

$$\eta(T) = 0.237 - 0.00046\ T \tag{B5}$$

The electrical output power may now be calculated by using Eqs. (B3) and (B5):

$$P = \eta(T) \frac{I}{r^2} \sin i$$

$$P = \frac{130}{r^2} \left[0.237 - \frac{0.1532}{\sqrt{r}} (\sin i)^{1/4} \right] \sin i \tag{B6}$$

The equation for the power may be rewritten by normalizing with respect to the maximum power ($i = \pi/2$) at 1.0 AU, P_o. Thus, if r has units of AU, then

$$G(r) \equiv \frac{P}{P_o} = \frac{2.825}{r^2} \sin i - \frac{1.825}{r^{2.5}} (\sin i)^{5/4} \tag{B7}$$

Solving $dG/dr = 0$ for $\sin i$ yields the optimum value of $\sin i$,

$$\begin{aligned} (\sin i)_{opt} &= 2.35\ r^2 \qquad (0 \le r \le 0.652) \\ (\sin i)_{opt} &= 1 \qquad\qquad (r > 0.652) \end{aligned} \tag{B8}$$

In addition there exists a lower limit on i. At angles less than the lower limit, the back side of the panel is exposed to solar flux (due to the finite size of the Sun), which causes the temperature to increase rapidly. The angle at which this occurs is given by $\tan i = R/r$,

where R is the radius of the Sun. By combining this expression with Eq. (B8), the radius at which this occurs is calculated to be 0.13 AU. Furthermore, fixing i at its lower limit causes G(r) to fall rapidly to zero at slightly less than 0.1 AU. Observing these limits on i and substituting Eq. (B8) into Eq. (B7) lead to the final form of the solar cell power profile (displayed in Fig. 3):

$$G(r) \begin{cases} \equiv 0 & (r \leq 0.13 \\ = 1.33 & (0.13 \leq r \leq 0.652) \\ = \dfrac{2.825}{r^2} - \dfrac{1.825}{r^{2.5}} & (0.652 \leq r) \end{cases}$$

It should be realized that this derivation is somewhat approximate for a number of reasons. For instance, experiments performed on silicon solar cells[17] indicate that cell efficiency depends on solar flux intensity and that both cell efficiency and absorptivity are also functions of the incidence angle i when i is less than about 40°. Also, performance degradation due to charged-particle irradiation[18] and the interaction between the spacecraft and the solar panels were also ignored. These effects are not as yet defined well enough to warrent inclusion in this preliminary analysis. The silicon solar cell power profiles appearing in Refs. 17 and 18 do not differ greatly from Fig. 3. In Ref. 18 gallium-arsenide solar cell power profiles were found to be considerably more favorable than those of silicon cells for close-in solar probes.

REFERENCES

1. Athay, R. Grant, and House, Lewis L., "Close in solar probe. Preliminary draft report of suggested experiments," NASA TM X-51877 (1963).
2. Matthews, Howard F., and Erickson, Myles D., "The NASA advanced pioneer mission," Paper 857D, SAE, (April 1964).
3. Dugan, Duane W., "A preliminary study of the solar-probe mission," NASA TN D-783 (1961).

4. Gobetz, Frank W., "Minimization of time for double impulse solar probe mission," ARS J., 32, 438-440 (1962).

5. Moyer, H. Gardner, "Minimum impulse coplanar circle-ellipse transfer," AIAA J., 3, 723-726 (1965).

6. Fimple, W. R., and Edelbaum, T. N., "Applications of SNAP-50 class powerplants to selected unmanned electric propulsion missions," Paper 64-494, Am. Inst. Aeron. and Astronaut. (June 1964).

7. d'Arcy, R. J., and Sinko, G. C., "Unmanned electric propulsion mission capabilities of the SNAP-50/SPUR powerplant," Connecticut Aircraft Nuclear Engine Lab., Pratt and Whitney Aircraft Div., United Aircraft Corp., Rep. PWAC-447 (October 1964).

8. Lundholm, J. G., Jr., Prohaska, E. S., Hoyer, S, and Averell, J., "A close approach solar probe design feasibility and mission study," Paper 64-496, Am. Inst. Aeron. and Astronaut. (June 1964).

9. Strack, W. C., "Combined high-low thrust propulsion for the close solar probe mission," NASA TN D-3145 (1965).

10. Ray, Kenneth A., and Winicur, Daniel H., "A large area solar cell array," Paper 64-739, Am. Inst. Aeron. and Astronaut. (September 1964).

11. Gordon, Gary D., "A 30 KW power supply from thin film solar cells," Paper 64-740, Am. Inst. Aeron. and Astronaut. (September 1964).

12. Ritchie, D., Toms, R., and Menetrey, W., "Potentials of solar power electric propulsion," Paper 66-210, Am. Inst. Aeron. and Astronaut. (March 1966).

13. Molitor, J. H., Berman, D., Seliger, R. L., and Olson, R. N., "Design of a solar-electric propulsion system for interplanetary spacecraft," Paper 66-214, Am. Inst. Aeron. and Astronaut. (March 1966).

14. Melbourne, W. G., "Interplanetary trajectories and payload capabilities of advanced propulsion vehicles," Jet Propulsion Lab., Calif. Inst. of Tech. Tech. Rept. 32-68 (March 1961).

15. MacKay, John S., and Rossa, Leonard G., "A variational method for the optimization of interplanetary round-trip trajectories," NASA TN D-1660 (1963).

16. Broder, J D., Kautz, H. E., Mandelkorn, J., Schwartz, L., and Ulman, R. P., "Solar-cell performance at high temperatures," NASA TN D-2529 (1965).

17. Johnston, P. A., "Laboratory experiments on the performance of silicon solar cells at high solar intensities and temperatures," NASA TN D-2733 (1965).

18. Staff of Electro-Electronic Division, "Application of Gallium-Arsenide Solar Cells to Solar Probe Power Systems," Radio Corp. Am. (February 1, 1966).

19. Todd, James P., and Sheets, Ronald E., "Development of a regeneratively cooled 30-KW arcjet engine," AIAA J., 3, 122-126 (1965).

20. Mickelsen, William R., "Electric propulsion," Space/Aeronautics, 42, 50-53 (1964).

21. Jack, John R., Spisz, Ernie W., and Brinich, Paul F., "Research on resistance-heated hydrogen thrustors," NASA TN D-2281 (1964).

22. Bennett, Stewart, Connors, John F., and Clark, Kenn E., "Development of a 3-kilowatt resistojet," Paper 64-672, Am. Inst. Aeron. and Astronaut. (August 1964).

23. Mickelsen, William R., and Kaufman, Harold R., "Status of Electrostatic Thrustors for Space Propulsion," NASA TN D-2172 (1964).

24. Reader, Paul D., "Experimental performance of a 50 centimeter diameter electron-bombardment ion rocket," Paper 64-689, Am. Inst. Aeron. and Astronaut. (August 1964).

25. Mickelsen, William R., and MacKay, John S., "Interplanetary flight with electric propulsion," Astronaut. and Aeronaut., 3, 44-49 (1965).

TABLE I. - ASSUMED CONSTANTS

Parameter	Assumed value
V_c, ft/sec	25 600
m_s/m_o	0.10
k	0.10 (electron-bombardment engines) 0.15 (electrothermal engines)
K[a]	0.137 (Saturn IB/Centaur) 0.447 (Atlas/Centaur)
I_c, sec[a]	420 (Saturn IB/Centaur) 440 (Atlas/Centaur)

[a]The values of K and I_c appearing in this table should not be taken as numbers corresponding to actual Centaur hardware. Instead, they are two parameters evaluated for a curve fit of the form given by Eq. (5) to Saturn IB/Centaur and Atlas/Centaur launch vehicle performance data.

TABLE II. - SYSTEM PERFORMANCE FOR 0.1 AU SOLAR FLYBY MISSION[a]

System	Mission time, T_M, days	Payload, lb	Power to thrustors, kW_e	Specific impulse of final stage, sec	High thrust burnout velocity, V_b, ft/sec
Saturn IB/Centaur/kick stage	75	0	----	444	67 000
Saturn IB/nuclear ($1\frac{1}{2}$ stages)	75	0	----	800	67 000
Saturn IB/Centaur/electric (constant power)	400 500	1050 2350	48.0 49.9	3900 4400	39 200 37 800
Saturn IB/Centaur/electric (solar cell power)	400 500	1310 1850	31.9 37.1	4100 4900	41 800 39 900
Atlas/Centaur/electric (solar cell power)	500	230	9.4	4700	37 600

[a]Saturn IB assumed to inject 32 000 lb payload into 100-n.mi. Earth orbit. Atlas/Centaur assumed to inject 10 800 lb payload into 100-n.mi. Earth orbit. Overall specific powerplant mass α = 75 lb/kW_e.

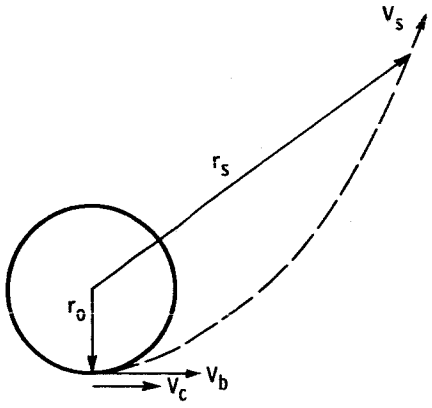

(a) Earth-centered escape maneuver.

(b) Heliocentric initial velocity V_0.

Fig. 1. - Orbital velocity diagram.

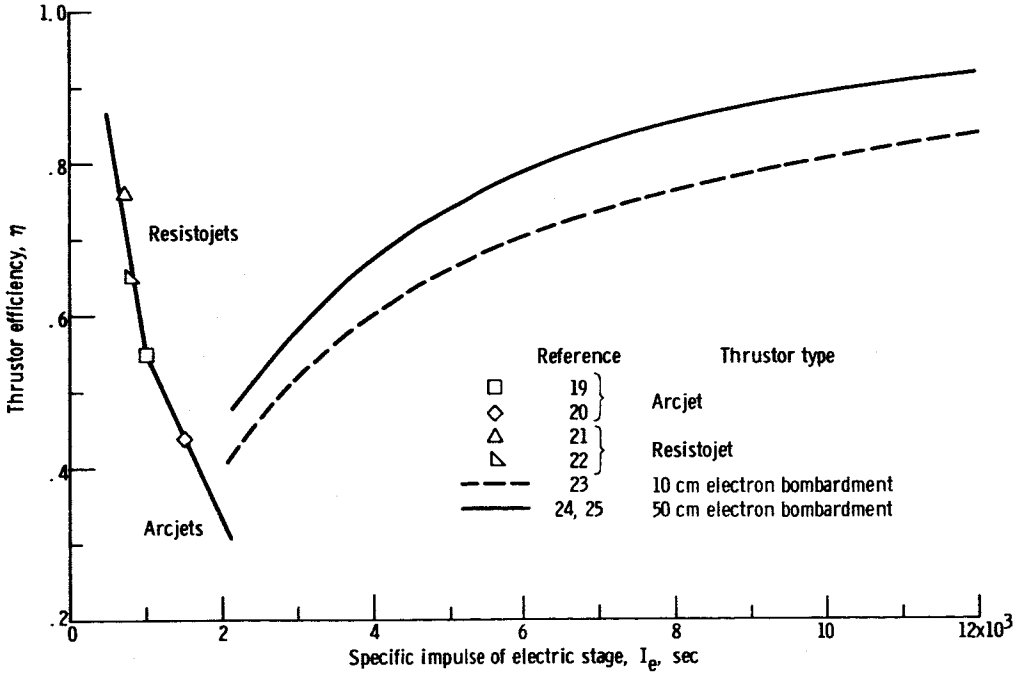

Fig. 2. - Assumed variation of thrustor efficiency as a function of specific impulse.

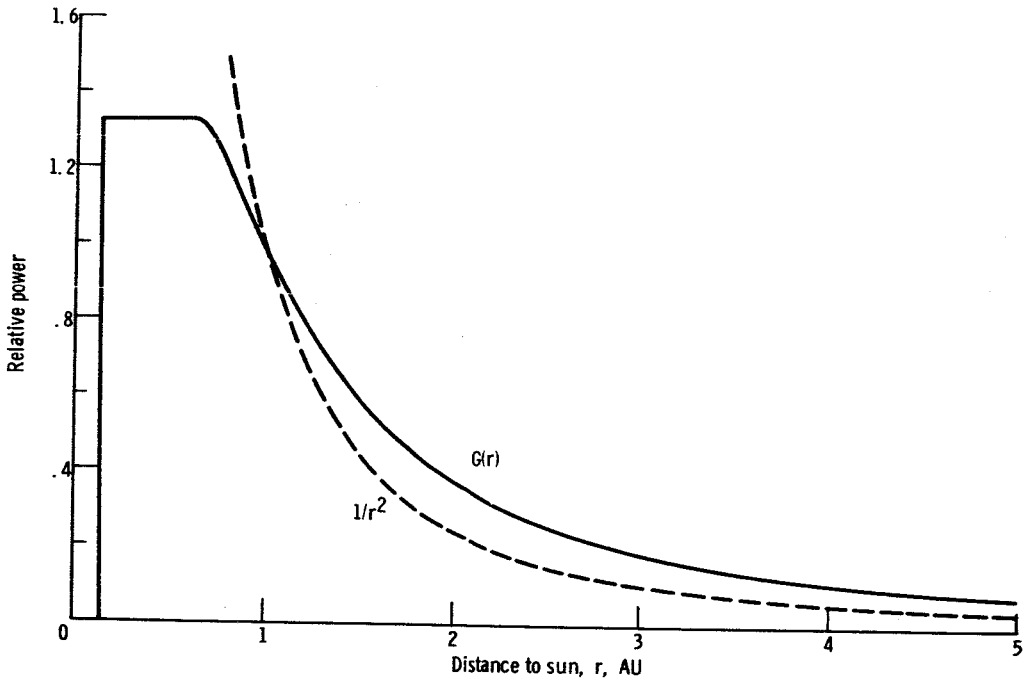

Fig. 3. - Silicon solar cell power profile.

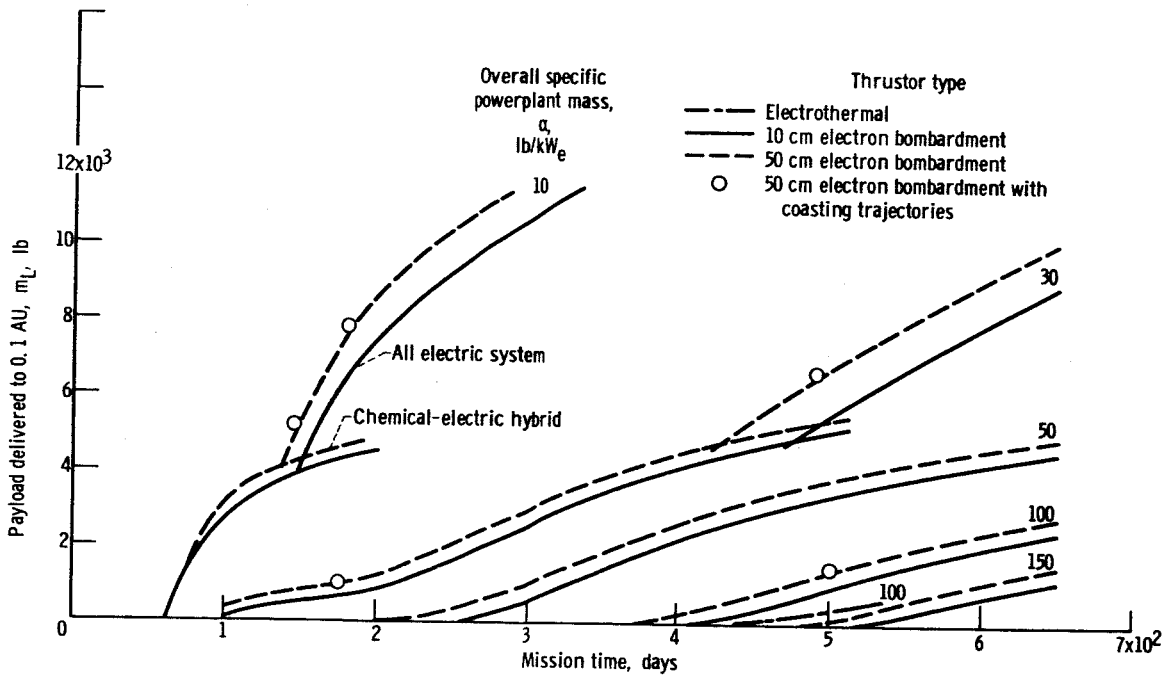

Fig. 4. - Payload delivered to 0.1 AU by Saturn IB/Centaur/electric system with constant power. Saturn IB assumed to insert 32 000 lb in 100 n. mi. Earth orbit.

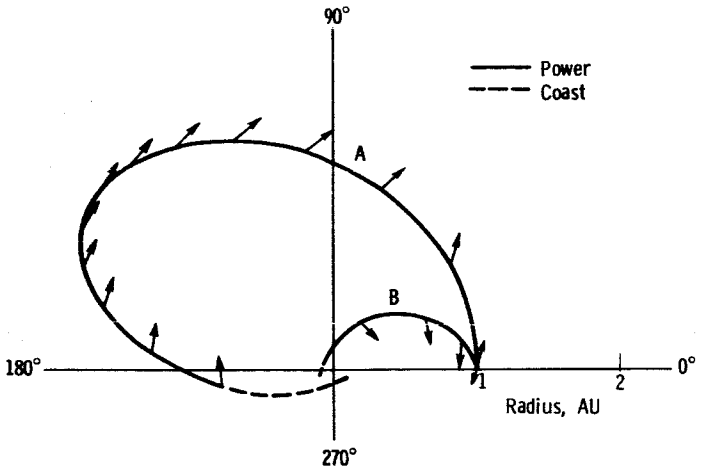

Trajectory	Mission time, days	α(lb/kW$_e$)	Thrust pointer interval, days
A	500	100	40
B	70	30	20

Fig. 5. - Two typical 0.1 AU solar fly-by trajectory diagrams for constant power hybrid system. Optimum V_b, I_e, θ, a_o.

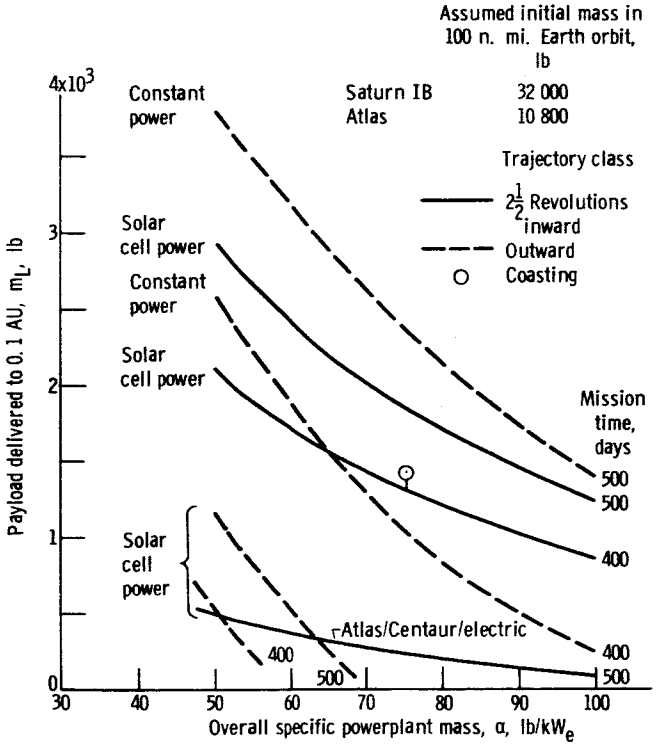

Fig. 6. - Payload delivered to 0.1 AU by Saturn IB/Centaur/electric vehicle using 50 cm electron bombardment engines.

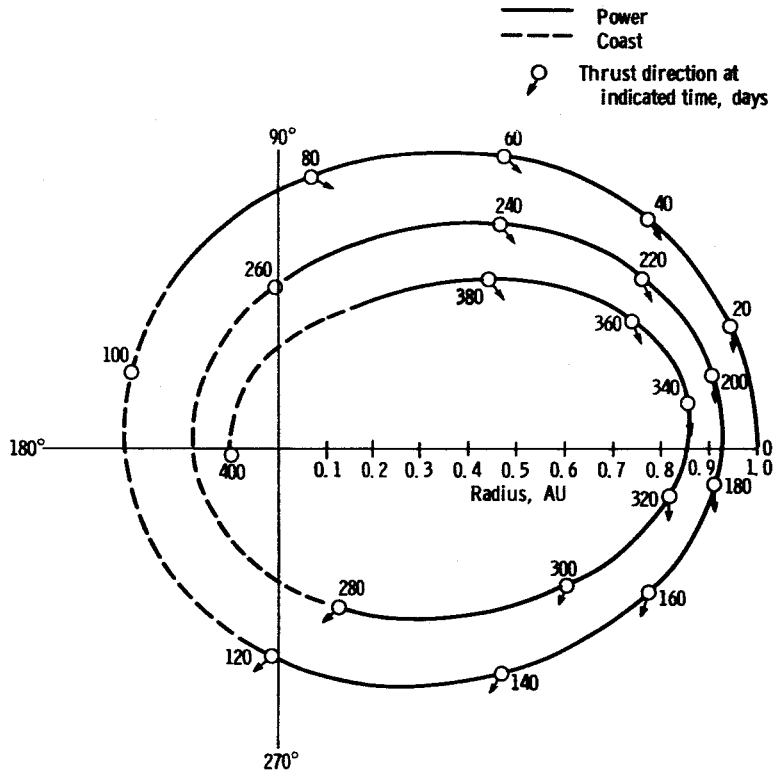

Fig. 7. - Typical 0.1 AU solar fly-by trajectory for 400-day mission using solar power hybrid system, $\alpha = 75$ lb/kW$_e$.